Using Contact Residual Responses of a 3-DOF Scooter to Identify First Few Frequencies of the Footbridge

Zhenkun Li(✉), Yifu Lan, and Weiwei Lin

Department of Civil Engineering, Aalto University, Espoo, Finland
zhenkun.li@aalto.fi

Abstract. Indirect identification of bridge modal parameters using vibrations of the passing vehicle has attracted much interest from researchers in the last two decades. In extant studies, the quarter- and half-car models are commonly employed, but apparent discrepancies can be noticed between these models and real cars. In addition, for a footbridge, classical vehicles may not be suitable for indirectly identifying its frequencies. Scooters, as common vehicles with unsophisticated dynamic structures, are widely available in daily life and can provide a new thought for indirect parameter identification of footbridges. As an initial investigation, this paper proposed a footbridge frequency identification strategy based on the collected vibrations of a passing scooter. The vibrations are collected by two accelerometers installed on the scooter's body and front wheel. To remove the frequencies of the scooter itself in the frequency domain, contact-point responses are back-calculated from its vibrations. Furthermore, the influence of the road roughness, as a key obstacle for identifying the footbridge's frequencies, is eliminated by employing residual contact-point responses of front and rear wheels, which makes the footbridge's frequencies outstanding in the frequency domain. The proposed idea is verified numerically by the scooter's finite element model with three degrees of freedom and a simply supported bridge model. The results indicate that the proposed method performs effectively and robustly when several influence factors are considered and shows great potential in practical applications.

Keywords: Footbridge · Frequency identification · Contact-point response · Scooters

1 Introduction

Bridge structures are playing important roles in current transportation systems. The safety of bridges has attracted much attention from scholars as the rapid increase of old bridges [1]. Among all bridges, a considerable number of them are footbridges. Modal parameters, as fundamental properties of bridges, are universally investigated for health monitoring purposes [2–4]. Traditionally, to obtain the vibration modes of the bridge, accelerometers are expected to attach to the bridge directly to collect its

M. P. Limongelli et al. (Eds.): EVACES 2023, LNCE 433, pp. 132–143, 2023.
https://doi.org/10.1007/978-3-031-39117-0_14

vibrations. However, some challenging problems were noticed when the method was applied in engineering. For example, it normally needs numerous sensors installed on the bridge in the construction stage, which is inevitably expensive and time-consuming. Besides, hazardous weather in special areas like Nordic countries may pose challenges for maintaining those sensors. Furthermore, this sensing system is typically prioritized for long or extremely important bridges. Footbridges are normally not on that list, but they can be hundreds of meters long and play significant roles in people's daily life [5]. As the number of existing bridges is increasing, developing a quick and reliable method to identify bridges' modal information is in great demand. In order to solve the above problems and meet the requirements of identifying modes of increasing amounts of bridges, the indirect method was proposed by Yang et al. in 2004 [6]. Typically, it only needs several sensors instrumented on the passing vehicle, making it economical and easy-to-operate when employed in engineering applications. Besides, since sensors are attached to the vehicle, it becomes easier to check, maintain, or repair them once some faults are found. After the idea was proposed, researchers were soon attracted by the indirect idea owing to its obvious advantages [7–9].

Previously, it had been verified that the bridge's natural frequencies, modal shapes, and damping ratios are contained in the accelerations of the passing vehicle [10, 11]. Natural frequencies, as the fundamental modal parameters of the bridge, were commonly explored. Initially, the vehicle's accelerations were utilized directly to identify the bridge's frequencies. Filter techniques, different vehicle parameters, and several connected vehicles were explored to highlight the bridge's frequencies in the vehicle's frequency-domain responses [12–14]. However, the accelerations of the vehicle could always contain information about the vehicle itself, making it difficult to pick the bridge's frequencies if the vehicle's frequencies were unknown beforehand. In order to remove the vehicle's frequencies in the frequency domain, the contact-point (CP) responses between the vehicle and bridge were back-calculated from the vehicle's vibrations [15]. Since CP responses were not relevant to the vehicle, vehicle frequencies can be completely removed in the frequency-domain spectrum. Further, to eliminate the inverse influence of road roughness, two connected vehicles or a two-axle vehicle experiencing the same road roughness were employed [16, 17]. However, currently, most studies employed quarter- or half-car models in simulations, and obvious discrepancies can be observed between these models and real cars. Besides, for footbridges, they cannot burden normal cars' weights, making it unachievable to apply car-based methods. Researchers have noticed that bicycles can be good tools for identifying the footbridge's parameters [18]. Scooters, as common vehicles with simple components, are widely available in daily life in many countries. They do not need tractors and can be driven independently, thus have the potential to provide a new thought for indirect parameter identification of footbridges. This paper employs the scooter to indirectly identify the footbridge's frequencies. Firstly, the scooter's FE model with three degrees of freedom (DOFs) is carefully built, and equations for back-calculating its CP responses are derived when tire damping is considered. Then, to eliminate the inverse influence of road roughness, the residual CP responses between the front and rear tires are utilized. Finally, the robustness of the proposed method is tested under several influence factors in engineering applications.

2 Simulation and CP Response Calculation

2.1 VBI Model

The scooter in Fig. 1a is simulated by the model as shown in Fig. 1b with three DOFs, and the bridge is simulated by a simply supported beam using beam elements. Compared with quarter- or half-car models that are employed to simulate real cars, the proposed model is consistent with the scooter.

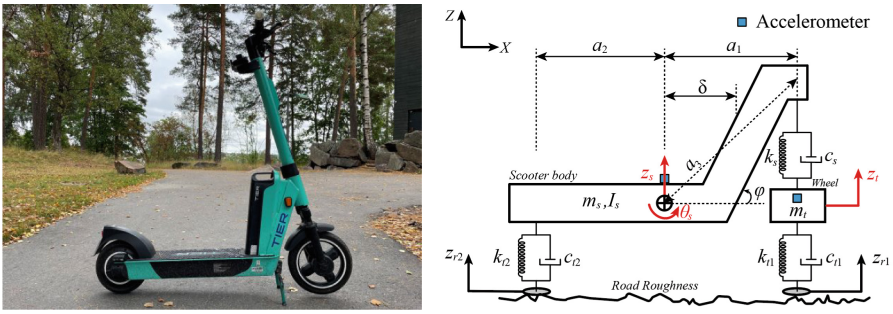

(a) Real scooter (b) FE model of the scooter

Fig. 1. Scooter and its FE model.

For the scooter, three DOFs are denoted by red arrows, as shown in Fig. 1b: vehicle body bounce z_s, body pitching θ_s, and bounce of the front wheel z_t. Two accelerometers are utilized to collect the scooter's translational and angular accelerations when passing the footbridge. The scooter body's mass is m_s, and its pitching moment of inertia is I_s. The mass of the front wheel is m_t. Since the rear wheel is tightly connected to the vehicle body and no suspension is employed for it, its mass is included in the scooter body. a_1, a_2, a_3, δ and φ are constants for determining the gravity center, and a_3 can be calculated by Eq. (1).

$$a_3 = \sqrt{((a_1 - \delta)\tan\varphi)^2 + (a_1)^2} \tag{1}$$

The stiffness and damping of the suspension system for the front wheel are represented by k_s, c_s, and the tire's stiffness and damping are denoted by k_{t1}, k_{t2}, c_{t2}, c_{t2}. The scooter's dynamic equilibrium equation is represented by Eqs. (2–4),

$$\begin{aligned} m_s\ddot{z}_s + c_s\left(\dot{z}_s + a_3\dot{\theta}_s - \dot{z}_t\right) + k_s(z_s + a_3\theta_s - z_t) + c_{t2}\left(\dot{z}_s - a_2\dot{\theta}_s - \dot{u}_{c2}\right) \\ + k_{t2}(z_s - a_2\theta_s - u_{c2}) = 0 \end{aligned} \tag{2}$$

$$\begin{aligned} I_s\ddot{\theta}_s + a_1c_s\left(\dot{z}_s + a_3\dot{\theta}_s - \dot{z}_t\right) + a_1k_s(z_s + a_3\theta_s - z_t) - a_2c_{t2}\left(\dot{z}_s - a_2\dot{\theta}_s - \dot{u}_{c2}\right) \\ - a_2k_{t2}(z_s - a_2\theta_s - u_{c2}) = 0 \end{aligned} \tag{3}$$

$$m_t\ddot{z}_t - c_s\left(\dot{z}_s + a_3\dot{\theta}_s - \dot{z}_t\right) - k_s(z_s + a_3\theta_s - z_t) + c_{t1}(\dot{z}_t - \dot{u}_{c1}) + k_{t1}(z_t - u_{c1}) = 0 \tag{4}$$

Equations (2–4) can be rewritten in the matrix format as shown in Eq. (5)

$$\mathbf{M}_s\ddot{\mathbf{z}}_s(\mathrm{t}) + \mathbf{C}_s\dot{\mathbf{z}}_s(t) + \mathbf{K}_s\mathbf{z}_s(t) = \boldsymbol{p}_s \tag{5}$$

where $\mathbf{M}_s$, $\mathbf{C}_s$ and $\mathbf{K}_s$ are the scooter's mass, damping, and stiffness matrices that can be found in Appendix. $\ddot{\mathbf{z}}_s(\mathrm{t})$, $\dot{\mathbf{z}}_s(t)$ And $\mathbf{z}_s(t)$ are acceleration, velocity, and displacement vectors of the scooter; $\boldsymbol{p}_s$ is the external excitation vector applied to the scooter. $\boldsymbol{p}_s$ And $\boldsymbol{z}_s$ can be calculated by Eq. (6),

$$\boldsymbol{p}_s = \begin{bmatrix} k_{t1}u_{c2} + c_{t1}\dot{u}_{c2} \\ a_2k_{t1}u_{c2} + a_2c_{t1}\dot{u}_{c2} \\ k_{t2}u_{c1} + c_{t2}\dot{u}_{c1} \end{bmatrix}, \boldsymbol{z}_s = \begin{bmatrix} z_s \\ \theta_s \\ z_t \end{bmatrix} \tag{6}$$

where u_{ci} is displacement at the i-th contact point and can be calculated by $u_{ci} = z_{ri} + u_{bi}, i = 1, 2.z_{ri}$ is the road roughness as introduced in Fig. 1b, and u_{bi} is the footbridge's deflection at the i-th contact point. z_{ri} and u_{bi} are illustrated in Fig. 2. The bridge is simply supported at each end, as shown in Fig. 2. It is divided into N^b beam elements, and there are two DOFs for each node. The bridge's vibration equations can be denoted by Eq. (7),

$$\mathbf{M}_b\ddot{\mathbf{z}}_b(\mathrm{t}) + \mathbf{C}_b\dot{\mathbf{z}}_b(t) + \mathbf{K}_b\mathbf{z}_b(t) = \boldsymbol{p}_b^N \tag{7}$$

where $\mathbf{M}_b, \mathbf{C}_b$ and $\mathbf{K}_b$ are the bridge's mass, damping, and stiffness matrices. The damping is simulated by the Rayleigh damping, which can be calculated by

$$\begin{cases} \mathbf{C}_b = b_0\mathbf{M}_b + b_1\mathbf{K}_b \\ b_0 = \frac{2f_{b1}f_{b2}}{f_{b1}+f_{b2}}\xi, b_1 = \frac{2}{f_{b1}+f_{b2}}\xi \end{cases} \tag{8}$$

where ξ represents the footbridge's first two order damping ratios $\xi = \xi_1 = \xi_2$. f_{b1} and f_{b2} are its first two frequencies, respectively. When the scooter is passing on the footbridge, if its tires are not on the footbridge's nodes exactly, the Hermitian cubic interpolation function is utilized to distribute the contact force to adjacent nodes. This process can be completed by Eqs. (9–12),

$$\boldsymbol{p}_b^N = \mathbf{N}_c\begin{bmatrix} k_{t1}(z_t - u_{c1}) + c_{t1}(\dot{z}_t - \dot{u}_{c1}) - m_sg \cdot a_2/(a_1 + a_2) - m_tg \\ k_{t2}(z_s - a_2\theta_s - u_{c2}) + c_{t2}\left(\dot{z}_s - a_2\dot{\theta}_s - \dot{u}_{c2}\right) - m_sg \cdot a_1/(a_1 + a_2) \end{bmatrix} \tag{9}$$

$$\mathbf{N}_c = \begin{bmatrix} 0 \cdots 0 & \cdots \boldsymbol{\lambda}_1 \cdots 0 \\ 0 \cdots \boldsymbol{\lambda}_2 \cdots 0 & \cdots 0 \end{bmatrix}^T \tag{10}$$

$$\boldsymbol{\lambda}_i = \left[1 - 3\zeta_i^2 + 2\zeta_i^3, \zeta_i^3 l - 2\zeta_i^2 l + \zeta_i l, 3\zeta_i^2 - 2\zeta_i^3, \zeta_i^3 l - \zeta_i^2 l\right] \tag{11}$$

$$\zeta_i = (x_i(t) - (\gamma - 1)l)/l \tag{12}$$

where $x_i(t)$ means the distance of the i-th contact points on the γ-th element to the bridge's left end, and l is the length of the bridge's element. The footbridge's deflections at nodes $\boldsymbol{z}_b$ can be obtained by employing the Newmark-β method. Furthermore, its deflection at contact points can be obtained by $\boldsymbol{u}_b = \mathbf{N}_c^T\boldsymbol{z}_b$, and the velocity can be obtained as $\dot{\boldsymbol{u}}_b = v(\mathbf{N}_c')^T\boldsymbol{z}_b + \mathbf{N}_c^T\dot{\boldsymbol{z}}_b$, in which $(')$ means the derivative to x, and $\dot{()}$ is the derivative to time t. The above calculation process can be executed several times until the footbridge's deflection between two iterations reaches an acceptable value.

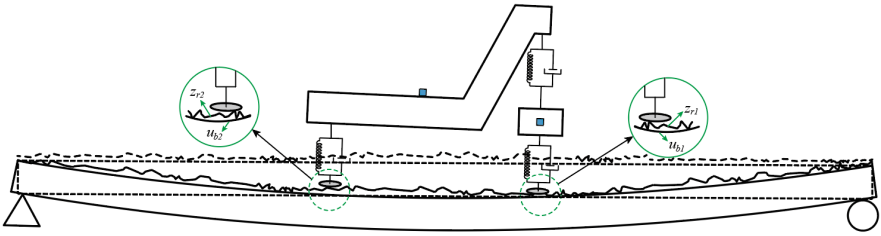

Fig. 2. Illustration of the scooter passing a footbridge.

2.2 Road Roughness

Road roughness can be simulated by the power spectral density (PSD) function in ISO 8608 [19] in this paper. The procedure can be represented by Eqs. (13) and (14),

$$r(x) = \sum_{i=1}^{N} \sqrt{2G_d(n_i)\Delta n}\cos(2\pi n_i x + \theta_i) \tag{13}$$

$$G_d(n_i) = G_d(n_0)(n_i/n_0)^{-2} \tag{14}$$

where $r(x)$ is the generated road roughness. θ_i is random number uniformly distributed between 0 and 2π. Δn is the sampling interval of the spatial frequency and is 0.01 cycle/m. n_0 is taken as 0.1 cycle/m, and n_i is set as numbers from 0.01 to 10 m^{-1} with an interval of $0.01m^{-1}$. $G_d(n_0)$ should be selected by the class of road roughness.

2.3 Back-Calculated CP Response

From Eq. (2–4), we can notice that all three equations are related to contact-point displacement u_{ci}. Specifically, u_{c1} is included in Eq. (4), and u_{c2} is included in Eq. (2) and (3). For calculating $\ddot{u}_{c1}$, by taking the second order derivative of Eq. (4) and rearranging items related to CP responses, we can get

$$\ddot{u}_{c1} + \frac{c_{t1}}{k_{t1}}\frac{d\ddot{u}_{c1}}{dt} = \mathrm{Q}_1(t) \tag{15}$$

$$\mathrm{Q}_1(t) = \frac{m_t}{k_{t1}}\frac{d^2\ddot{z}_t}{dt^2} - \frac{c_s}{k_{t1}}\left(\frac{d\ddot{z}_s}{dt} + a_3\frac{d\ddot{\theta}_s}{dt} - \frac{d\ddot{z}_t}{dt}\right) - \frac{k_s}{k_{t1}}\left(\ddot{z}_s - a_3\ddot{\theta}_s - \ddot{z}_t\right) + \frac{c_{t1}}{k_{t1}}\frac{d\ddot{z}_t}{dt} + \ddot{z}_t \tag{16}$$

It can be noticed that Eq. (15) is a first-order linear differential equation, and it can be solved analytically. In Eq. (16), all differentials can be numerically calculated by first-order finite difference formulas and second-order central formulas, as shown in Eq. (17) and (18).

$$\frac{dZ}{dt} = \frac{Z(s) - Z(s-1)}{\Delta t} \tag{17}$$

$$\frac{d^2Z}{dt^2} = \frac{Z(s+1) - 2Z(s) + Z(s-1)}{(\Delta t)^2} \tag{18}$$

The above process can also be employed for calculating $\ddot{u}_{c2}$. However, Eqs. (17) and (18) will inevitably introduce some errors because approximate numerical computations.

Therefore, minimizing calculating errors needs also be considered. We noticed that there are many similar items in Eq. (2) and (3). By taking $a_1 \times Eq.(2) - Eq.(3)$, we can get Eq. (19). For Eq. (19), the same process is employed to obtain $\ddot{u}_{c2}$. Results are shown in Eq. (20) and (21),

$$a_1 m_s \ddot{z}_s - I_s \ddot{\theta}_s + (a_1 + a_2) c_{t2} \left(\dot{z}_s - a_2 \dot{\theta}_s - \dot{u}_{c2} \right) + (a_1 + a_2) k_{t2} (z_s - a_2 \theta_s - u_{c2}) = 0 \tag{19}$$

$$\ddot{u}_{c2} + \frac{c_{t2}}{k_{t2}} \frac{d\ddot{u}_{c2}}{dt} = \mathrm{Q}_2(t) \tag{21}$$

$$\mathrm{Q}_2(t) = \frac{a_1 m_s}{(a_1+a_2)k_{t2}} \frac{d^2 \ddot{z}_s}{dt^2} - \frac{I_s}{(a_1+a_2)k_{t2}} \frac{d^2 \ddot{\theta}_s}{dt^2} - \frac{c_{t2}}{k_{t2}} \left(\frac{d\ddot{z}_s}{dt} + a_2 \frac{d\ddot{\theta}_s}{dt} \right) + \ddot{z}_s - a_2 \ddot{\theta}_s \tag{22}$$

In the above equations, m_s, m_t, c_s, k_s, c_{ti}, k_{ti}, a_1, a_2 and a_3 can be measured in experiments. $\ddot{z}_s$, $\ddot{\theta}_s$ and $\ddot{z}_t$ are collected accelerations when the scooter passes the footbridge. Solving Eq. (15) and (20), Eq. (22) is obtained. Because in practice, the accelerations are collected discretely, by transforming the integration into summation, we can obtain Eq. (23),

$$\ddot{u}_{ci}(t) = \begin{cases} \mathrm{Q}_i(t), i = 1, 2. \ if \ \ c_{ti} = 0 \\ \frac{k_{ti}}{c_{ti}} \exp\left(-\frac{k_{ti}}{c_{ti}} t \right) \left(\int_0^t \mathrm{Q}_i(\tau) \exp\left(\frac{k_{ti}}{c_{ti}} \tau \right) d\tau \right), i = 1, 2., \ \ if \ \ c_{ti} \neq 0 \end{cases} \tag{22}$$

$$\ddot{u}_{ci}(t) = \begin{cases} \mathrm{Q}_i(t), i = 1, 2. \ if \ \ c_{ti} = 0 \\ \frac{k_{ti}}{c_{ti}} \left(\sum_{j=1}^{t/\Delta t} \mathrm{Q}_i |_j \exp\left(\frac{k_{ti}}{c_{ti}} (j\Delta t - t) \right) \Delta t \right), i = 1, 2; j = 1, 2, \ldots \ if \ \ c_{ti} \neq 0 \end{cases} \tag{23}$$

where $\Delta t = 1/f_s$, and f_s is the sampling frequency. j means the j-th sampling point of the vehicle's accelerations.

3 Simulation Results and Discussions

3.1 Parameters of the VBI System

In this section, parameters in Table 1 are utilized for simulation the VBI system.

The scooter's speed is 5 m/s (18 km/h), which is a slightly lower than its maximum speed (20 km/h) and easy to keep in practical applications. The distance between its two wheels is 0.92 m, and the gravity center position can be determined by $a_1 = 0.42$ m and $a_2 = 0.5$ m. Employing the above parameters, the scooter's frequencies can be obtained as $f_{s1} \sim f_{s3}$. There are ten elements for the footbridge, and an accelerometer is attached to the bridge for comparison reasons, as shown in Fig. 3. The sampling frequency for the scooter and bridge is 1 kHz.

For road roughness, $G_d(n0) = 4e^{-6}$ m^3 is employed to generate an A-class road profile. Due to the tire contact with the road, the original road roughness is smoothed accordingly [20].

Table 1. Basic parameters of the vehicle and bridge.

VBI	Parameters	Value
Scooter	Scooter body mass (m_s)	111.2 kg
	Scooter body moment of inertia ($I_{v\theta}$)	101.5 kg · m^2
	Front wheel mass (m_t)	1.17 kg
	Suspension damping (c_s)	2000 N · s/m
	Tire damping (c_{t1}, c_{t2})	0, 0 N · s/m
	Suspension stiffness (k_s)	13067 N/m
	Tire stiffness (k_{t1}, k_{t2})	8×10^4, 8×10^4 N/m
	Constants ($a_1, a_2, \delta, \varphi$)	0.42, 0.50, 0.15 m, $7\pi/18$ rad
	Velocity (v)	5 m/s
	Scooter frequencies (f_{s1}, f_{s2}, f_{s3})	1.48, 4.93, 44.8 Hz
Footbridge	Length (L)	30 m
	Flexural stiffness (EI)	1.746×10^8 N/m^2
	Mass per unit length ($\overline{m}$)	40 kg/m
	Bridge frequencies (f_{b1}, f_{b2}, f_{b3})	3.64, 14.58, 32.83 Hz

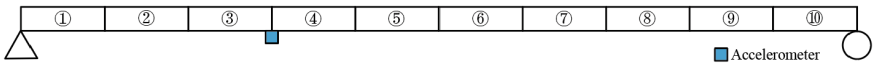

Fig. 3. FE model of the footbridge.

3.2 Simulation Results

In this section, the scooter's vibrations will be investigated at first. Since road roughness is the most important factor influencing the identification of the footbridge's frequencies, two scenarios: (1) No road roughness, and (2) A-class road roughness, are discussed in this section. Then, a more realistic example is introduced, which considers more factors when the proposed method is utilized in engineering applications.

No Road Roughness. To verify the proposed back-calculation equations for CP responses using the scooter's vibrations, influence factors, such as environmental noises, footbridge damping, and tire damping, are temporarily ignored and will be discussed in the section: More Realistic Study.

It can be seen from Fig. 4b that the footbridge's first three frequencies can be clearly identified when the road roughness is not considered. However, amplitudes at the second and third order frequencies are relatively low compared to the first frequency. For the scooter's body responses, it is hard to recognize the second and third frequencies as they

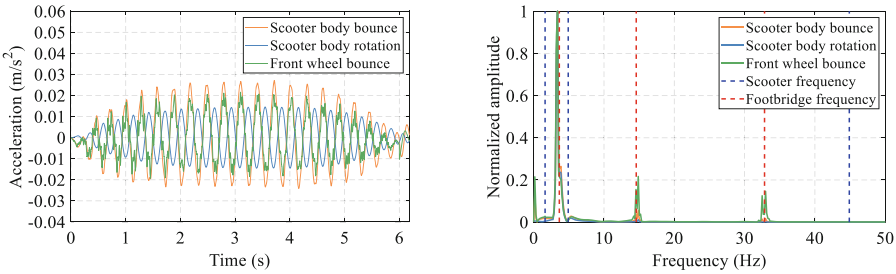

(a) Vibrations of the scooter (b) FFT of the scooter's vibrations

Fig. 4. Vibrations and FFT spectrum of the scooter.

are too weak. The reason for this is that because there is no road roughness, the scooter is not fully excited, making the footbridge's responses relatively low.

A-Class Road Roughness. If the A-class road is employed, the simulation results are shown in Fig. 5. It can be seen that due to the influence of road roughness, only the first frequency can be observed if the scooter body's angular acceleration is employed. We can see the overwhelming effect of road roughness in masking the bridge frequencies of the higher modes.

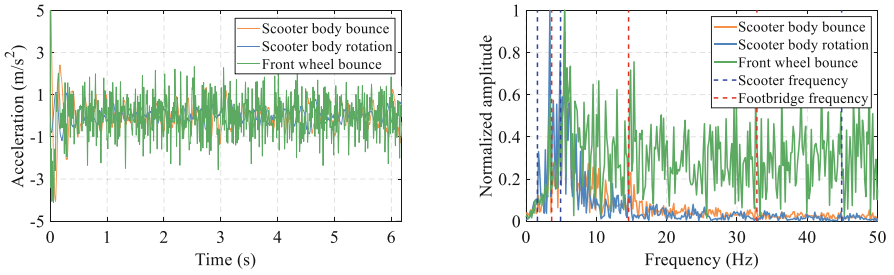

(a) Vibrations of the scooter (b) FFT of the scooter's vibrations

Fig. 5. Vibrations and FFT spectrum of the vehicle.

The scooter's CP responses are merely related to the bridge's deflection and road roughness, thus having the potential to identify the footbridge's frequencies. The scooter's CP responses can be back-calculated by Eq. (23). Since for the simulation, we already know the road roughness (in engineering, it is unknown), the true CP responses can be obtained by the road profile and the footbridge's accelerations. The comparison of calculated and true CP responses for the front wheel is shown in Fig. 6. To observe the accelerations clearly, only CP responses in the first 1 s are plotted. From Fig. 6, we can see that the calculated CP responses are very close to the true ones, which verifies the equations back-calculating CP responses from the scooter's vibrations. However, due to the influence of road roughness, the footbridge's frequencies are submerged in the frequency domain.

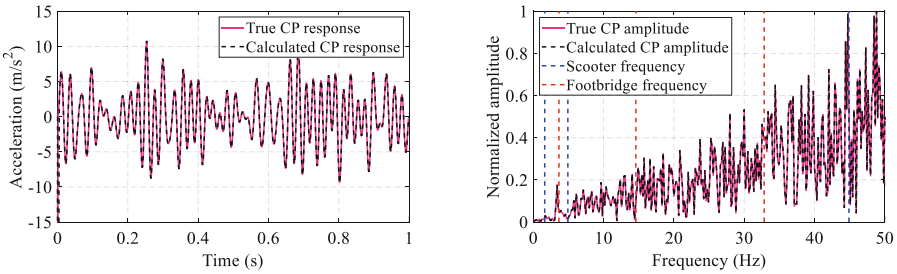

(a) CP responses (b) FFT amplitudes of CP responses

Fig. 6. CP responses and FFT amplitudes.

Because the front and rear wheels will experience the same road roughness with a time lag, to solve the above problem, the residual CP responses between the front and rear wheels are utilized to eliminate the inverse influence of road profile. The time lag can be calculated by Eq. (24),

$$T_{lag} = (a_1 + a_2)/v \tag{24}$$

By subtracting the CP responses of the rear wheel from the front one at the same road profile point, the residual CP response and its spectrum are shown in Fig. 7.

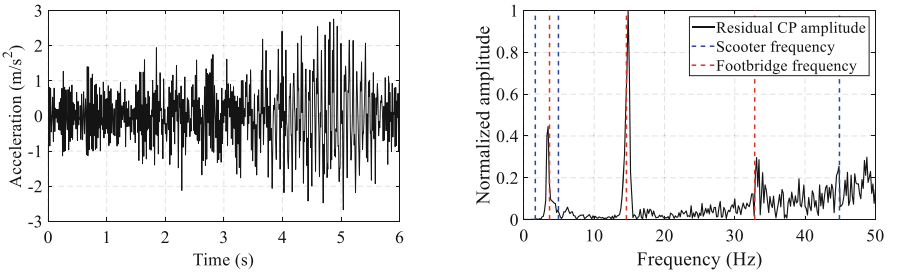

(a) Residual CP responses (b) FFT amplitudes of residual CP responses

Fig. 7. Residual CP responses and FFT amplitudes.

We can see from Fig. 7b that the influence of road roughness has been removed in the frequency domain. The footbridge's frequencies are easy to be identified.

More Realistic Study. In the last sections, only the road roughness is considered. However, in engineering applications, there will be more factors that can impact the identification of the footbridge's frequencies. In this section, the following factors are considered: (1) environmental noises, (2) footbridge damping, and (3) scooter tire damping. For the environmental noise, it is simulated by Eq. (25),

$$\ddot{z}_{noise} = \ddot{z} + E_p N_s \sigma_{\ddot{z}} \tag{25}$$

where N_s is random numbers subject to the normal distribution, and $\sigma_{\ddot{z}}$ is the standard deviation of the scooter's accelerations. For the footbridge's damping, it is assumed that

$\xi = 0.02$. The scooter's tire damping is set as $c_{t1} = c_{t2} = 1\text{kN} \cdot \text{s/m}$. The identification results using residual CP responses are shown in Fig. 8. It can be seen that the footbridge's third frequency is masked in high-frequency range when environmental noises, footbridge damping, and tire damping are considered. The first two frequencies remain identifiable, which verifies the robustness of the proposed method.

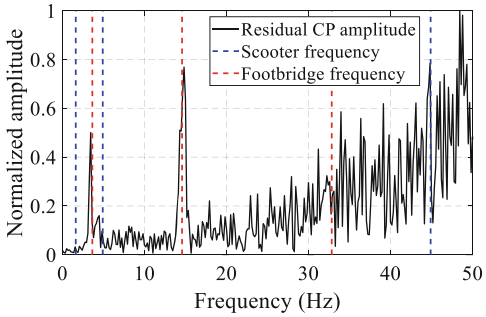

Fig. 8. Practical example of footbridge frequency identification.

4 Conclusions and Future Studies

In this paper, an indirect footbridge frequency identification method using an ordinary scooter's vibrations is proposed. The scooter's FE model with three DOFs is carefully built, and the simply supported footbridge is simulated by beam elements. To eliminate the scooter self-frequencies and inverse effects of road roughness, residual CP responses are employed. Several concluding remarks are drawn below:

(1) The road roughness can inversely influence identifying the footbridge's frequencies. When road roughness is not considered, the footbridge's frequencies can be directly determined from the scooter's vibrations; however, those frequencies will be submerged when there is road roughness.
(2) Since the CP response is only related to the footbridge's responses and road roughness, it has nothing to do with the scooter itself, making the scooter self's frequencies disappear in the frequency domain. Calculating residual CP responses between the front and rear tires can eliminate the inverse effects of road roughness.
(3) Environmental noises, footbridge damping, and tire damping mainly affect the high-frequency range (>20 Hz in this study), and the identification of low order frequencies (first two frequencies in this study) of the footbridge is rarely influenced.

Even though the footbridge's frequencies can be identified under several different conditions, more influence factors, such as scooter speeds and walking pedestrians, deserve further studies. Our future study will be extended to check the above factors in identifying the footbridge's frequencies before engineering applications.

Acknowledgements. This research is financially sponsored by the Jane and Aatos Erkko Foundation in Finland (Decision number: 210018). Y. Lan is also financially supported by the Finnish Foundation for Technology Promotion (TES) and Chinese Scholarship Council (CSC).

Appendix

$$\mathbf{M}_s = \begin{bmatrix} m_s & 0 & 0 \\ 0 & I_s & 0 \\ 0 & 0 & m_t \end{bmatrix}, \mathbf{C}_s = \begin{bmatrix} c_s + c_{t2} & a_3 c_s - a_2 c_{t2} & -c_s \\ a_1 c_s - a_2 c_{t2} & a_1 a_3 c_s + a_2^2 c_{t2} & -a_1 c_s \\ -c_s & -a_3 c_s & c_s + c_{t1} \end{bmatrix}$$

$$\mathbf{K}_s = \begin{bmatrix} k_s + k_{t2} & a_3 k_s - a_2 k_{t2} & -k_s \\ a_1 k_s - a_2 k_{t2} & a_1 a_3 k_s + a_2^2 k_{t2} & -a_1 k_s \\ -k_s & -a_3 k_s & k_s + k_{t1} \end{bmatrix}$$

References

1. Zhang, Y., Yuen, K.V.: Review of artificial intelligence-based bridge damage detection. Adv. Mech. Eng. **14**, 1–21 (2022)
2. Hou, R., Xia, Y.: Review on the new development of vibration-based damage identification for civil engineering structures: 2010–2019. J. Sound Vib. **491**, 115741 (2021)
3. Li, Z., Hou, J., Jankowski, Ł: Structural damage identification based on estimated additional virtual masses and Bayesian theory. Struct. Multidiscip. Optim. **65**(2), 1–18 (2022)
4. Hou, J., Li, Z., Zhang, Q., et al.: Optimal placement of virtual masses for structural damage identification. Sensors (Switzerland) **19**, 1–18 (2019)
5. Dallard, P., Fitzpatrick, A.J., Flint, A., et al.: The London millennium footbridge. Struct. Eng. **79**, 17–21 (2001)
6. Yang, Y.B., Lin, C.W., Yau, J.D.: Extracting bridge frequencies from the dynamic response of a passing vehicle. J. Sound Vib. **272**, 471–493 (2004)
7. Wang, Z.L., Yang, J.P., Shi, K., et al.: Recent advances in researches on vehicle scanning method for bridges. Int. J. Struct. Stab. Dyn. **22**, 2230005 (2022)
8. Li, Z., Lin, W., Zhang, Y.: Real-time drive-by bridge damage detection using deep autoencoder. Structures **47**, 1167–1181 (2023)
9. Li, Z., Lin, W., Zhang, Y.: Drive-by bridge damage detection using Mel-frequency cepstral coefficients and support vector machine. Struct. Heal Monit. **00**, 147592172211509 (2023)
10. Malekjafarian, A., Corbally, R., Gong, W.: A review of mobile sensing of bridges using moving vehicles: Progress to date, challenges and future trends. Structures **44**, 1466–1489 (2022)
11. Siringoringo, D.M., Fujin, Y.: Estimating bridge fundamental frequency from vibration response of instrumented passing vehicle: analytical and experimental study. Adv. Struct. Eng **15**, 417–433 (2012)
12. Yang, Y.B., Chang, K.C., Li, Y.C.: Filtering techniques for extracting bridge frequencies from a test vehicle moving over the bridge. Eng. Struct. **48**, 353–362 (2013)
13. Shi, Z., Uddin, N.: Extracting multiple bridge frequencies from test vehicle – a theoretical study. J. Sound Vib. **490**, 115735 (2021)
14. Kong, X., Cai, C.S., Kong, B.: Numerically extracting bridge modal properties from dynamic responses of moving vehicles. J. Eng. Mech. **142**, 04016025 (2016)

15. Yang, Y.B., Zhang, B., Qian, Y., Wu, Y.: Contact-point response for modal identification of bridges by a moving test vehicle. Int. J. Struct. Stab. Dyn. **18**, 1850073 (2018)
16. Yang, Y.B., Mo, X.Q., Shi, K., et al.: Scanning torsional-flexural frequencies of thin-walled box girders with rough surface from vehicles' residual contact response: theoretical study. Thin-Walled Struct. **169**, 108332 (2021)
17. He, Y., Yang, J.P.: Using acceleration residual spectrum from single two-axle vehicle at contact points to extract bridge frequencies. Eng. Struct. **266**, 114538 (2022)
18. Quqa, S., Giordano, P.F., Limongelli, M.P.: Shared micromobility-driven modal identification of urban bridges. Autom. Constr. **134**, 104048 (2022)
19. ISO 8608. Mechanical vibration—Road surface profiles—Reporting of measured data. E:44 (2016)
20. Xu, H., Liu, Y.H., Wang, Z.L., et al.: General contact response of two-mass single-axle test vehicles for scanning bridge frequencies considering suspension effect, 270 (2022)